Earthq Eng & Eng Vib (2008) 7:147-163 **DOI**: 10.1007/s11803-008-0835-6

Simplified approach for design of raft foundations against fault rupture. Part I: free-field

I. Anastasopoulos[1,2†], N. Gerolymos[1†], G. Gazetas[1‡] and M. F. Bransby[2§]

1. *School of Civil Engineering, National Technical University of Athens, Greece*

2. *Civil Engineering, University of Dundee, Scotland, UK*

Abstract: Over the past few decades, earthquake engineering research mainly focused on the effects of strong seismic shaking. After the 1999 earthquakes in Turkey and Taiwan, and thanks to numerous cases where fault rupture caused substantial damage to structures, the importance of faulting-induced deformation has re-emerged. This paper, along with its companion (Part II), exploits parametric results of finite element analyses and centrifuge model testing in developing a four–step semi–analytical approach for analysis of dip-slip (normal and thrust) fault rupture propagation through sand, its emergence on the ground surface, and its interaction with raft foundations. The present paper (Part I) focuses on the effects of faulting in the absence of a structure (i.e., in the free-field). The semi-analytical approach comprises two-steps: the first deals with the rupture path and the estimation of the location of fault outcropping, and the second with the tectonically-induced displacement profile at the ground surface. In both cases, simple mechanical analogues are used to derive simplified semi-analytical expressions. Centrifuge model test data, in combination with parametric results from nonlinear finite element analyses, are utilized for model calibration. The derived semi-analytical expressions are shown to compare reasonably well with more rigorous experimental and theoretical data, thus providing a useful tool for a first estimation of near-fault seismic hazard.

Keywords: fault rupture; semi-analytical expression; soil-structure interaction; earthquake

1 Introduction

In an earthquake, damage can arise not only from the oscillatory shaking of the ground (the result of a multitude of inciting waves) but also from the permanent displacement ("offset") of the seismogenic fault itself, whenever its rupture emerges on the ground surface. A few notable historical examples: The 1891 Mino-Owari (Nobi) earthquake in Japan with a fault offset of up to 8 m (Matsuda, 1974), the 1906 San Francisco earthquake in USA with a fault offset of up to 6 m (Segall & Lisowski, 1990), the 1939 Erzincan North Anatolian earthquake in Turkey with an offset of up to 8 m (Bernard *et al*., 1997), the 1988 Armenia earthquake with an offset of up to 2 m (Philip *et al*., 1992), and the 1990 Luzon earthquake in Philippines with an offset of up to 5 m (Nakata *et al*., 1996), etc.

Recently, in 1999, three destructive earthquakes in Turkey (Kocaeli and Düzce) and Taiwan (Chi-Chi), offered a variety of case histories of surface fault rupturing with many civil engineering structures on top. This has re-fuelled the interest on the subject, giving a new perspective to the not-so-new idea that a structure could survive a surface fault rupture (Duncan & Lefebvre, 1973; Berill, 1983; Youd, 1989). To this end, an integrated approach has been applied in the course of a European research project (QUAKER), comprising: (i) field studies of documented case histories, (ii) geotechnical centrifuge experiments, and (iii) finite element analyses (Anastasopoulos & Gazetas, 2007a, 2007b; Anastasopoulos *et al*., 2007a, 2007b; Bransby *et al*., 2007a, 2007b; Faccioli *et al*., 2007). The latter were validated through successful genuine (blind) Class "A" predictions (Lambe, 1973) against the results of experimental model tests.

This paper, along with its companion (Anastasopoulos *et al*., 2008), exploit the results of this effort and develop a four-step simplified approach for analysis of dip-slip (normal and thrust) fault rupture propagation through sand and its interaction with raft foundations. The problem studied herein is illustrated schematically in Fig. 1, along with the four steps of the developed methodology. We consider a uniform soil deposit of thickness H, at the base of which a dip-slip (normal or reverse) fault, dipping at angle α, ruptures and produces bedrock offset of vertical

Correspondence to: G. Gazetas, 36 Asimakopoulou Str., Ag. Paraskevi 15342, Athens, Greece
Tel: (30) 210 600 85 78; Fax: (30) 210 772 24 05
E-mail: gazetas@ath.forthnet.gr
†Lecturer; ‡Professor; §Senior Lecturer

Supported by: OSE (the Greek Railway Organization), and the EU Fifth Framework Programme Under Grant No. EVG1-CT-2002-00064
Received March 23, 2008; **Accepte**d April 24, 2008

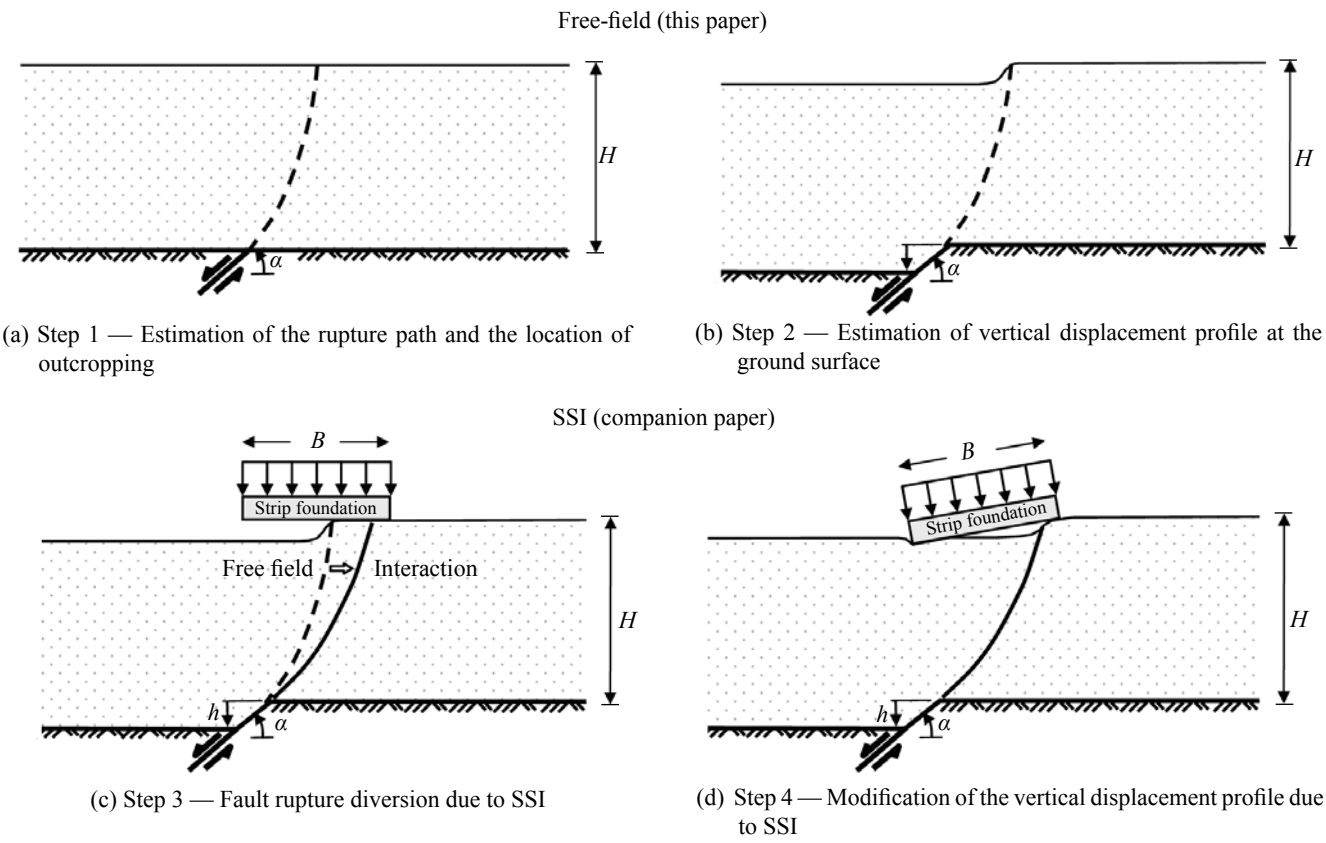

(a) Step 1 — Estimation of the rupture path and the location of outcropping

(b) Step 2 — Estimation of vertical displacement profile at the ground surface

(c) Step 3 — Fault rupture diversion due to SSI

(d) Step 4 — Modification of the vertical displacement profile due to SSI

Fig. 1 Problem definition and the four steps of the simplified semi-analytical approach

amplitude h.

A strip foundation of width B, carrying a uniformly distributed load q, interacts with the outcropping fault rupture and the deforming soil mass. The first two steps of the methodology deal with fault rupture propagation in the free-field, emphasizing on parameters of engineering significance, such as : (a) the location of fault outcropping (Step 1), and (b) the vertical displacement profile at the ground surface (Step 2). The last two steps, presented in the companion paper, deal with soil-structure interaction (SSI): (c) fault rupture diversion due to SSI (Step 3), and (d) modification of the vertical displacement profile due to SSI (Step 4).

2 Location of fault outcropping

Assuming that the location of a fault at bedrock is known, the location of "break-out" at the ground surface is related to the propagation of the rupture through the overlying soil deposit. The latter depends on a number of factors, including the style and magnitude of faulting, and the material characteristics of the overlying soils (Roth *et al*., 1982; Cole & Lade, 1984; Lade *et al*., 1984; Bray, 1990; Bray *et al*., 1994; Nakai *et al*., 1996; and Lee & Hamada, 2005). Fault rupture propagation has been analyzed in Anastasopoulos *et al*. (2007a; 2007b) through nonlinear finite element (FE) modeling. Analysis results were shown to be in agreement with centrifuge model tests, and the validity of the modelling methodology was demonstrated through successful Class "A" predictions. Normal faults were shown to refract at the soil−bedrock interface, and keep increasing in dip while approaching the surface, as a function of the friction angle φ and the dilation ψ. Similarly, reverse faults also refract at the soil−bedrock interface, but tend to decrease in dip approaching the surface. FE and centrifuge modelling results are utilized herein to develop a semi–analytical approach for the estimation of the rupture path, and the outcropping location.

2.1 Normal faulting

As depicted in Fig. 2, normal faulting can be seen as mechanically analogous to a gravity wall under active conditions (i.e. the soil is in an active state with a vertical major principal stress). Hence, a reasonable assumption is that the initial propagation dip angle α_{ini} will be in the direction of the stress characteristics :

$$\alpha_{ini} = 45^{o} + \varphi/2 \tag{1}$$

If the soil exhibited no dilation (i.e. $\psi = 0$), the rupture would outcrop at:

$$W_{o} = H / \tan(45^{o} + \varphi/2) = H \tan(45^{o} - \varphi/2) \tag{2}$$

where H is the depth of the soil slayer. For a normalized

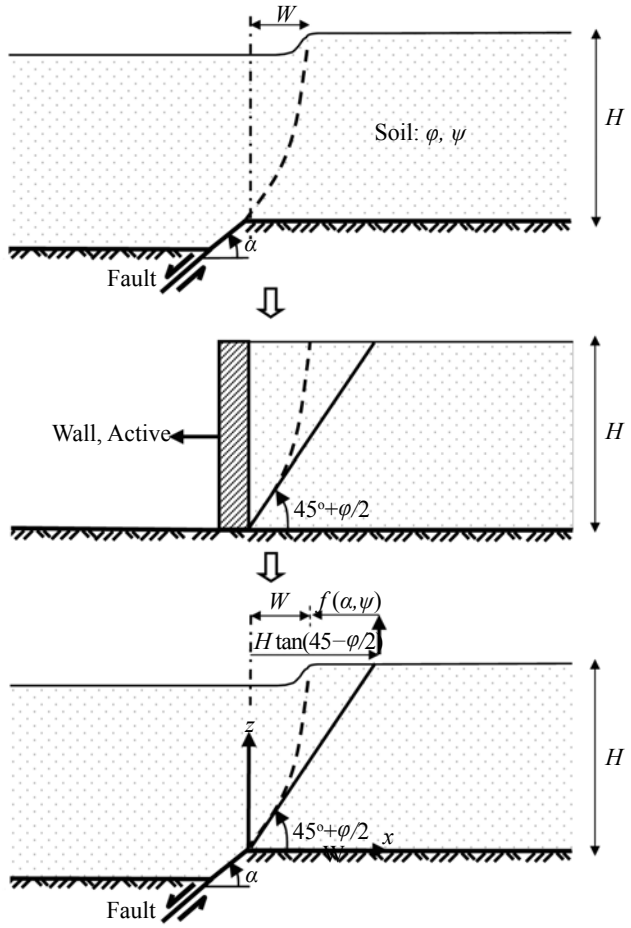

Fig. 2 Semi-analytical model for estimation of the rupture path as function of φ and ψ: analogy of normal faulting to a gravity wall under active conditions

height z/H (z measured from the bedrock interface), the normalized horizontal distance of the rupture path x/H will be :

$$\frac{x}{H} = \frac{z}{H} \tan(45^o - \varphi/2) \tag{3}$$

However, this rupture path is not straight as given in Eq.(3). Instead, for dilating soil (i.e., $\psi > 0$), the rupture bends over the hanging wall so that the rupture becomes steeper (increased dip angle) as the surface is approached. To incorporate such effects, Eq.(3) must be modified to allow for dilation. This contradicts the theoretical argument that the rupture path depends on the stress characteristics, but is required to give an empirical fit to the observed response. An additional empirical term is added to take account for the bedrock dip angle α. The final empirical expression of the non-dimensional rupture path account for both the dip angle and the angle of dilation:

$$\frac{x}{H} = \frac{z}{H} \tan(45^o - \varphi/2) \exp\left(\frac{1}{\cos(\pi - \alpha)} \frac{9}{2\pi^2} \tan(\psi) \frac{z}{H} \right) \tag{4}$$

where the term $9/2\pi^2 = 0.46$ is obtained through calibration against the results of FE analysis. Thus, the approach bases the dip angle at the soil base α_{ini} on the theoretical direction for an active shear zone, and allows deviation from this path through the soil based on empirical relationships with the dilation angle ψ and the bedrock dip angle α. The non-dimensional outcropping location can then be estimated through Eq.(4) setting $z = H$:

$$\frac{W}{H} = \tan(45^o - \varphi/2) \exp\left(\frac{1}{\cos(\pi - \alpha)} \frac{9}{2\pi^2} \tan(\psi) \right) \tag{5}$$

For $\alpha \le 45^o + \psi/2$, a secondary antithetic rupture also develops (Lade *et al*., 1984), initially propagating at an angle of $45^o + \varphi/2$ to the horizontal, but without substantial bending. Its non-dimensional propagation path is :

$$\frac{x}{H} = \frac{z}{H} / \tan(45^o + \varphi/2) = \frac{z}{H} \tan(45^o - \varphi/2) \tag{6}$$

Finally, the non-dimensional width of the associated graben can be estimated as follows:

$$\frac{W_G}{H} = \tan(45^o - \varphi/2) \left[1 + \exp\left(\frac{1}{\cos(\pi - \alpha)} \frac{9}{2\pi^2} \tan(\psi) \right) \right] \tag{7}$$

2.2 Thrust faulting

Thrust faulting could be seen as mechanically analogous to a gravity wall under passive conditions. However, with the exception of shallow faulting angles, $\alpha \le 30^o$, such an assumption cannot explain the observed values of α_{ini}, that tend to be closer to $45^o + \varphi/2$. Following the work of Prucha *et al*. (1965), we assume that vertical uplifting is the dominating mechanism when the fault is steep, $\alpha \ge 45^o$ (Fig. 3).

For a steep thrust fault, an analogy can be drawn to the Riedel Shear experiment (Tchalenko, 1970). As shown in Fig. 4, if we notionally rotate the shear apparatus by 90^o, the similarity with a steep reverse fault is clear. Riedel shears, which can be seen analogous to the initiation of fault rupture propagation, are oriented at $45^o + \varphi/2$ to the horizontal.

To the above initial dip angle ($\alpha_{ini} = 45^o + \varphi/2$), the effect of dilation ψ (the rupture will bend over the footwall with $\psi > 0$) and of the dip angle α can be added as for normal faults. Thus, the non-dimensional rupture path can be approximated empirically as:

$$\frac{x}{H} = \frac{z}{H} \tan(45^o - \varphi/2) \exp\left(\cos(\alpha) \frac{3\pi}{2} \tan(\psi) \frac{z}{H} \right) \tag{8}$$

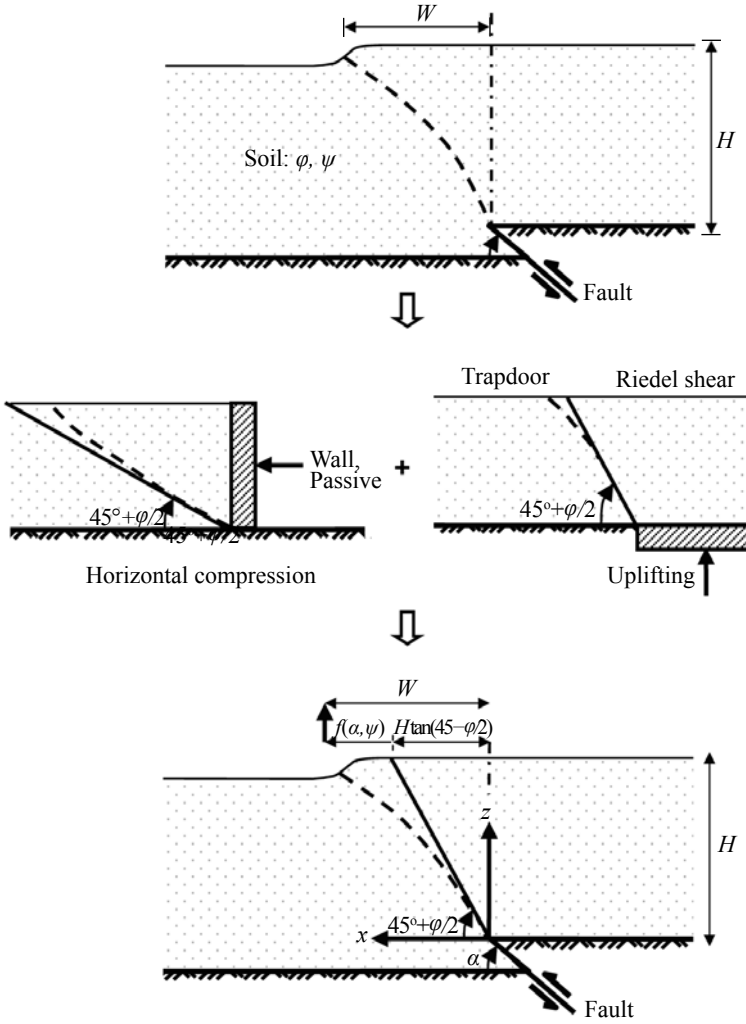

Fig. 3 Semi-analytical model for estimation of the rupture path as function of φ and ψ : analogy of *thrust* faulting to combination of a gravity wall under passive conditions and vertical uplifting

R: Riedel shear
R': Conjugate riedel shear
W: Shear zone width

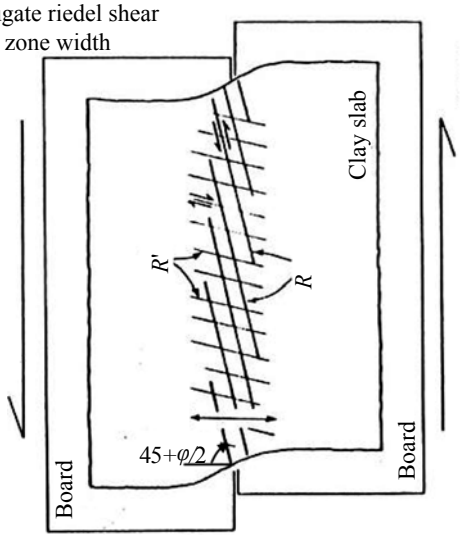

Fig. 4 The riedel shear experiment of Tchalenko (1970) and its analogy with the mechanism of the initiation of fault rupture propagation in reverse faulting

where the term $3\pi/2 = 4.71$ is obtained also through calibration against the results of FE analyses. The non-dimensional outcropping location can then be estimated setting $z = H$ as:

$$\frac{W}{H} = \tan(45^{o} - \varphi/2)\exp\left(\cos(\alpha)\frac{3\pi}{2}\tan(\psi)\right) \quad (9)$$

2.3 Results and discussion

The derived semi-analytical relationships are utilized to estimate fault rupture propagation paths for normal and reverse faulting at $\alpha = 45^{o}$ and 60^{o}. The estimation is performed for two idealized sands (Anastasopoulos *et al*., 2007a), and for the Fontainebleau sand (Gaudin, 2002) at a relative density $D_r = 60\%$ as used in centrifuge model tests. The main soil properties of the three sands are taken as follows: (a) dense sand: $\varphi = 45^{o}$, $\psi = 18^{o}$; (b) loose sand: $\varphi = 32^{o}$, $\psi = 3^{o}$; and (c) Fontainebleau sand: $\varphi = 39^{o}$, $\psi = 11^{o}$.

As mentioned previously, FE results were used for calibration of the semi-analytical relationship. Hence, the comparison with (a) and (b) can be seen as a verification of the semi-analytical model, while the comparison with (c) can be viewed as an independent prediction. The non-dimensional rupture paths are presented in Figs. 5 and 6, for α = 45º and 60º, respectively. The non-dimensional outcropping location W/H is plotted as a function of the fault dip angle α in Fig. 7. The semi-analytical relations are in good agreement with FE results, as expected. Additionally, the comparison against experimental data is also quite reasonable.

3 Vertical displacement profile at the ground surface

Outcropping dip-slip fault ruptures generate vertical and horizontal displacements at the ground surface. Notwithstanding the importance of horizontal deformation, in this study we focus on the estimation of the vertical displacement profile. As shown in Anastasopoulos *et al*. (2007a), up to imposed bedrock offset h_y/H the soil near the surface deforms quasi-elastically. Then, the rupture outcrops and most of the additional displacement is concentrated within a narrow zone. Hence, we divide the ground displacement into: (a) quasi-elastic, and (b) plastic. The quasi-elastic deformation (before fault outcropping) is estimated based on the logic of tunneling–induced displacements. The plastic deformations (i.e. the fault scarp) are estimated following a shear-zone oriented approach.

3.1 Quasi-elastic displacements

As schematically illustrated in Fig. 8, the quasi-elastic deformation of the ground surface of a soil layer of depth H subjected to dip-slip faulting, can be seen to be analogous to the settlement trough of a tunnel excavation at depth $z = H$. In the latter case, the shape of the settlement trough is idealized as a bell-shaped Gaussian curve (Peck, 1969). The width of the settlement trough can be estimated through a parameter i, representing the distance between the point of inflection and the tunnel axis:

$$S(x) = S_{\max} \exp\left(-\frac{x^2}{2i^2}\right) \tag{10}$$

where $S_{\max}$ is the maximum settlement, estimated by dividing the volume loss V with the width of the settlement trough:

$$S_{\max} = V / 2.5i \tag{11}$$

In tunneling, the values for i are related to the diameter of the tunnel. Hence, these recommendations cannot be applied directly to dip-slip faulting.

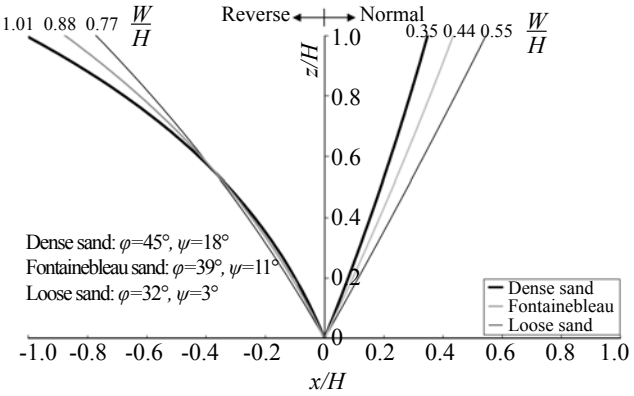

Fig. 5 Semi-analytical estimation of non-dimensional rupture paths, for α = 45º

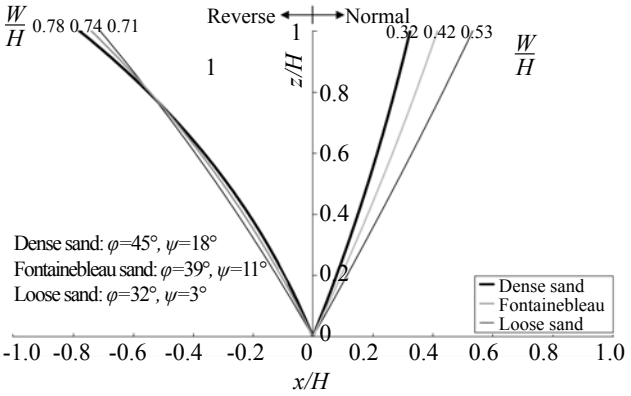

Fig. 6 Semi-analytical estimation of non-dimensional rupture paths, for α = 60º

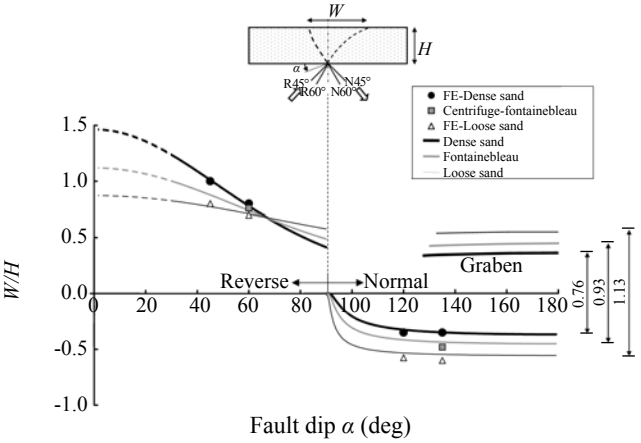

Fig. 7 Semi-analytical estimation of the rupture path: comparison between theoretical values of the non-dimensional fault outcropping location, *W/H*, with FE and centrifuge model test results.

Figure 9 depicts the vertical displacement profile and the angular distortion λ calculated using FE analysis plotted against horizontal distance from the point of application of the fault offset, for a normal α = 60º fault on loose sand. To "isolate" the quasi-elastic

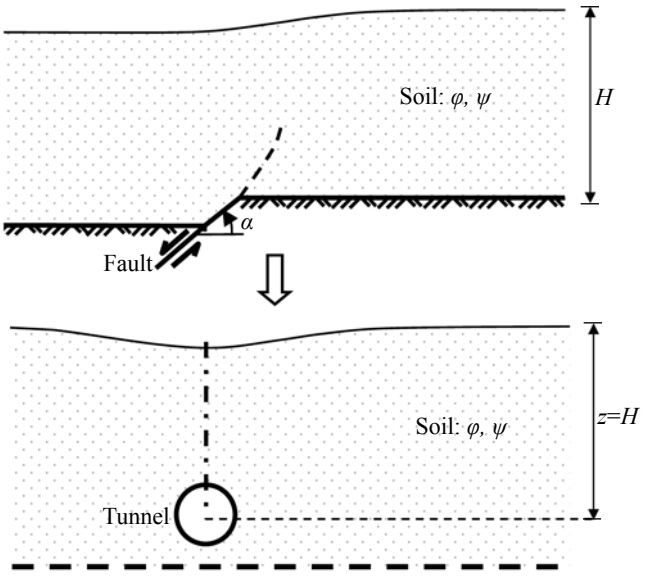

Fig. 8 Mechanical analogy of the quasi-elastic surface displacement produced by a dip slip fault on a soil layer of thickness *H* with the surface depression due to tunnel excavation at depth *z* = *H*

component of soil deformation, we plot the results for very small imposed fault offset: h/H = 0.25% (i.e., h = 0.1 m). Compared to tunnel-induced displacements, three distinct differences can be observed. First, if the distance from the point of inflection to the point of maximum settlement (or uplifting, for thrust faulting) at the left is i, then the distance from the same point to the point of minimum settlement at the right should be $\left(\sqrt{2\pi}-1\right)i \approx 1.5i$. However, we observe that the displacement profile is a little smoother to the right of the point of inflection, since the point of inflection is at a distance of the order of $2i$ instead of $1.5i$ from the un-deformed ($\lambda = 0$) zone, making the overall settlement trough wider and equal to a breadth of $3i$ (instead of $2.5i$).

A second difference is the magnitude of i, which is estimated to be in the order of $1.0H$ for the case of fault rupture propagation, a value larger than the suggested by Rankin (1988), $i = 0.5\,H$, for a tunnel at a depth $z = H$.

Finally, the third and most important difference is the location of the point of inflection and that of the point of maximum settlement. The former is at a distance x_p, which depends on the material type (dense or loose sand), the fault dip angle α, and the fault style (normal or reverse).

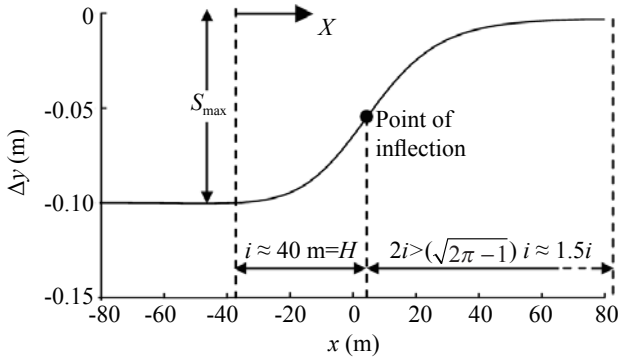

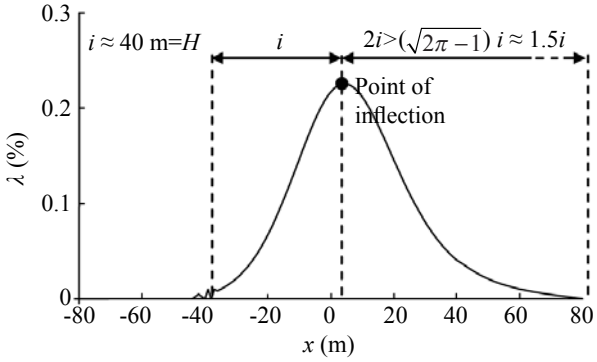

Fig. 9 Vertical displacement Δ*y* and distortion angle *λ* computed with FE analysis (normal faulting at *α* = 60^{o} through an *H* = 40m loose sand deposit) for small values of imposed offset *h/H* = 0.25%. The derived value of *i* is of the order of 1.0*H*

Let us now examine the evolution of the FE computed quasi-elastic angular distortion λ with the increase of the bedrock fault offset h/H. As illustrated in Fig. 10, the increase of h/H leads to a shifting of the points of inflection. This phenomenon is due to the inclined propagation of the fault rupture. As schematically illustrated in Fig. 11, for given h/H the tip of the propagating rupture will be at horizontal distance $x_p = f(\alpha, \varphi, \psi, h/H)$, which can be estimated using the semi-analytical relationship of the rupture path. At this point, the "equivalent" tunnel can be considered to lie at a depth (taking the middle of the traveled distance): $H - z_p/2$, and therefore the settlement trough will become narrower:

$$i = H - z_p/2 \tag{12}$$

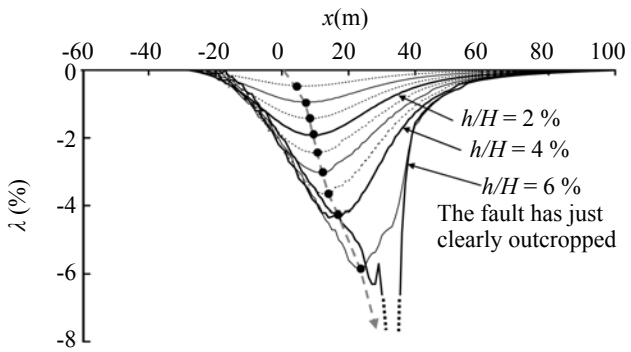

Fig. 10 Distortion angle *λ*, as computed from FE analysis (thrust faulting on loose sand at 60^{o}), showing the evolution of the location of inflection points with the increase of *h/H*

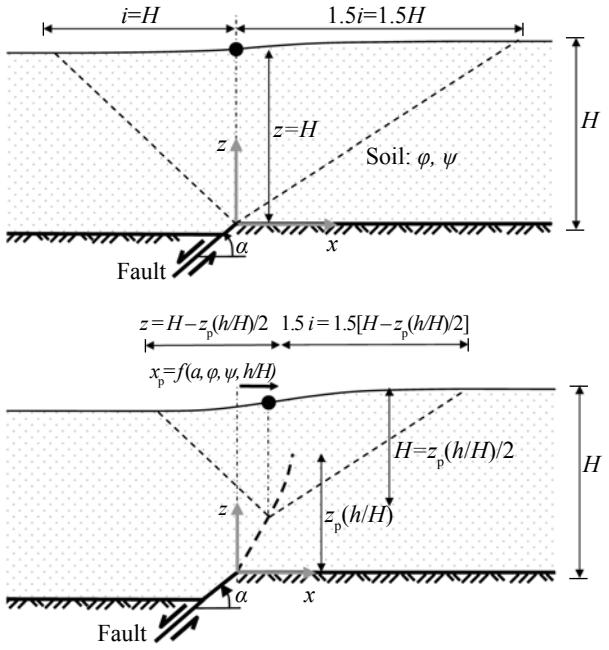

Fig. 11 Methodology to estimate the evolution of the point of inflection and the width of the displacement trough, with respect to the imposed bedrock offset *h/H*

For a given combination of fault style, α, φ, and ψ , there is a limiting value of offset h_y/H for which the fault outcrops at the surface (e.g., Bray, 1990 and Anastasopoulos *et al*., 2007a). We make a simplifying assumption that the non-dimensional propagation distance z_p/H is linearly related to h_y/H, as follows:

$$z_p / H = \frac{h/H}{h_y/H} \tag{13}$$

Thus, the non-dimensional rupture path is estimated to be a function of the imposed bedrock offset h/H :

$$\frac{x_p}{H} = \frac{h/H}{2h_y/H} \tan(45^o - \varphi/2) \bullet \exp\left(\frac{1}{\cos(\pi-\alpha)} \frac{9}{2\pi^2} \tan(\psi) \frac{h/H}{2h_y/H} \right) \tag{14}$$

for normal faulting, and

$$\frac{x_p}{H} = \frac{h/H}{2h_y/H} \tan(45^o - \varphi/2) \bullet \exp\left(\cos(\alpha) \frac{3\pi}{2} \tan(\psi) \frac{h/H}{2h_y/H} \right) \tag{15}$$

for thrust faulting.

Denoting $\hat{h} = h/H$, $\hat{h}_y = h_y/H$, and $\hat{x}_p = x_p/H$ the above equations can be written in a more convenient form:

$$\hat{x}_p = \frac{\hat{h}}{2\hat{h}_y} \tan(45^o - \varphi/2) \exp\left(\frac{1}{\cos(\pi-\alpha)} \frac{9}{2\pi^2} \tan(\psi) \frac{\hat{h}}{2\hat{h}_y} \right) \tag{16}$$

for normal faulting, and

$$\hat{x}_p = \frac{\hat{h}}{2\hat{h}_y} \tan(45^o - \varphi/2) \exp\left(\cos(\alpha) \frac{3\pi}{2} \tan(\psi) \frac{\hat{h}}{2\hat{h}_y} \right) \tag{17}$$

for thrust faulting.

In the same manner, Eq. (12) can be written in a non-dimensional form:

$$\hat{i} = 1 - \hat{h}/2\hat{h}_y \tag{18}$$

We now assume that each infinitesimal applied vertical displacement $d\hat{h}$ is responsible for creation of a bell-shaped settlement trough of maximum settlement $d\hat{h}$ and geometrical characteristics ($\hat{i}$, $\hat{x}_p$) as defined in Eq. (10). Then, the total non-dimensional quasi-elastic vertical displacement profile can be derived by integrating the settlement troughs of the infinitesimal imposed displacements $d\hat{h}$, i.e., an addition of an infinite number of bell-shaped Gaussian curves :

$$\hat{S}_e(\hat{x}, \hat{h}_e) = \int_0^{\hat{h}_e} \exp\left(- \frac{(\hat{x} + \hat{i} - \hat{x}_p)^2}{2 \cdot \hat{i}^2} \right) d\hat{h} \tag{19}$$

where $0 \le \hat{h}_e \le \hat{h}_y$ is the fraction of the maximum quasi-elastic displacement $\hat{h}_y$ for which the settlement trough is to be computed, $\hat{x} = x/H$, and $\hat{S} = S/h_y$. Substituting Eq. (16) for normal and Eq. (17) for thrust faulting in Eq. (19), we derive the quasi-elastic component of the vertical displacement for any non-dimensional bedrock offset $0 \le \hat{h}_e \le \hat{h}_y$:

$$\hat{S}_e(\hat{x}, \hat{h}_e) = -\int_0^{\hat{h}_e} \exp\left(- \frac{\left[\hat{x} + \left(1 - \frac{\hat{h}}{2\hat{h}_y} \right) - \frac{\hat{h}}{2\hat{h}_y} \tan(45^o - \varphi/2) \exp\left(\cos(\pi-\alpha)^{-1} \frac{9}{2\pi^2} \tan(\psi) \frac{\hat{h}}{2\hat{h}_y} \right) \right]^2}{2\left[1 - \frac{\hat{h}}{2\hat{h}_y} \right]^2} \right) d\hat{h} \tag{20}$$

for normal faulting, and

$$\widehat{S}_{\mathrm{e}}(\hat{x},\hat{h}_{\mathrm{e}})=\int_0^{\hat{h}_{\mathrm{e}}}\exp\left(-\frac{\left[\hat{x}+\left(1-\frac{\hat{h}}{2\hat{h}_{\mathrm{y}}}\right)-\frac{\hat{h}}{2\hat{h}_{\mathrm{y}}}\tan(45^{\mathrm{o}}-\varphi/2)\exp\left(\cos(\alpha)\,\frac{3\pi}{2}\tan(\psi)\,\frac{\hat{h}}{2\hat{h}_{\mathrm{y}}}\right)\right]^2}{2\left[1-\frac{\hat{h}}{2\hat{h}_{\mathrm{y}}}\right]^2}\right)\mathrm{d}\hat{h} \tag{21}$$

for thrust faulting.

Typical values of the non-dimensional critical bedrock offset for fault outcropping $\hat{h}_{\mathrm{y}}$, estimated on the basis of FE and centrifuge model test data, are given in Table 1.

Table 1 Typical values of the non-dimensional critical bedrock offset for fault outcropping $\hat{h}_{\mathrm{y}}$ (%) as a function of sand type and faulting style

	Loose $D_{\mathrm{r}}<35$ %	Medium–dense $D_{\mathrm{r}}=35\%-65$ %	Dense $D_{\mathrm{r}}=65\%-85$ %	Very Dense $D_{\mathrm{r}}>85$ %
Normal	> 1.5	1.25	0.75	< 0.75
Reverse	> 6	4	2.5	< 2.5

3.2 Plastic displacements

The plastic displacement trough refers to the localized inelastic deformation that takes place at the location of the fault outcrop. It is at least *two orders of magnitude narrower* than the quasi-elastic displacement trough. Its thickness depends on several factors, including the fault style, soil properties, and the magnitude of the bedrock fault offset. According to geological studies (e.g., Sibson, 2003), the thickness of the slip zone ranges from a few centimetres to tens of meters near the surface, decreasing to an order of millimeters at great depths, in which case it is mainly relevant with the mechanics of the rock mass: polishing of the fault surfaces (slickensides), solution transfer (coating of the surface with slickenfibers), cataclastic comminution, heat generation and melting processes, and hydrothermal fluid discharging. This study focuses on the mechanics of fault rupture propagation through granular soil, and therefore the investigation of such phenomena is not within our scope of work.

Several functions may be utilized to approximate the "plastic" displacement trough. Lazarte (1996) proposed four such functions and studied their applicability to the total displacement due to strike-slip faulting. A statistical methodology was utilized to achieve reasonable fit, recommending, however, that the results should be used in conjunction with empirical correlations of fault offset versus Moment Magnitude (Wells & Coppersmith, 1994). The approach presented herein is different: (a) while the methodology of Lazarte refers to the total displacement trough at the surface, in this work the displacement trough is divided into quasi-elastic and plastic; and (b) instead of curve fitting FE or field data, a simplified model is developed, with geotechnically meaningful parameters. A sigmoidal function is utilized to estimate the plastic displacement profile:

$$S_{\mathrm{p}}(x)=\tanh\left(\frac{2\pi}{T}x\right) \tag{22}$$

where T is a parameter controlling the width of the plastic settlement zone, referring to the thickness of the plasticized zone. We use the term *plasticized zone*, to denote the difference with the slip line (i.e. the shear band/localization).

The latter has been measured to be of the order of $10d_{50}$ to $20d_{50}$ (with d_{50} referring to the average particle size) in sands (Roscoe, 1970; Vardoulakis *et al*., 1985; and Muir Wood, 2002), and of the order of $200d_{50}$ in clays (Morgenstern & Tchalenko, 1967). A substantial difference between the two measurements lies in the experimental procedure used in each case: plane-strain and biaxial testing for sands, and direct-shear testing for clays. Without underestimating the shortcomings of the direct shear test (Hvorslev, 1960) and the inherent differences between sands and clays, we consider the tests by Morgenstern & Tchalenko (1967) of particular interest. Although the final shear band was macroscopically observed to be of the order of $200d_{50}$, through the microscope it was observed to consist of a family of discontinuities (smaller shear bands), of the order of $10d_{50}$ to $20d_{50}$. It is not straightforward to deduce which of the discontinuities should be considered as the shear band. Perhaps the whole phenomenon should be approached theoretically, such as by the fractal mechanics.

Attempting to answer such questions is not within the scope of this paper. However, it is appropriate to mention some of the scaling issues involved. While for the Kaolin clay, used in the direct shear tests

of Morgenstern *et al.* (1967), d_{50} = 0.5 μ, for a fine grained sand of $d_{50} \approx 300$ μ. Biaxial tests on sand are traditionally conducted using specimens on the order of 150 mm, meaning that the size of the specimen is about $500d_{50}$. So, from a scaling point-of-view, to yield an equivalent shear band estimation the Kaolin clay should be ideally tested in a miniature biaxial apparatus of $500d_{50} = 250\mu$. If such testing were possible, then the thickest observable shear band would indeed be of the order of $20d_{50}$: the macroscopic $200d_{50}$ shear band could not possibly fit in such an apparatus. On the other hand, to conduct an equivalent (from a scaling point-of-view) direct shear test on sand, an enormous direct shear apparatus would be required, of the order of $10000d_{50}$ in dimension (i.e., about 3 m for a fine grained sand).

To the best of our knowledge, such experiments have not yet been attempted, with the only exception being nature itself. For example, in the 1968 M_s 7.2 Dasht-e Bayaz earthquake in northern Iran, an array of Riedel shears in alluvium was observed quite systematically: at 30 m depth (observed from the inside of an underground aqueduct) the slip zone was on the order of 10 cm (Sibson, 2003). Palaeoseismic trenching investigations for different fault types indicate that at some depth within soil the deformation is usually localized in shear zones on the order of 10 cm in width (McCalpin, 1996). Similarly, in the 1992 Landers earthquake rupturing was localized within a shear zone of less than 50 cm in width (Lazarte *et al*., 1994). Such values tend to be closer to a $200d_{50}$ assumption, rather than the traditional $10d_{50}$ to $20d_{50}$ of the shear band. Therefore, for faulting-induced deformations, we consider a realistic value of the shear zone width, t_f:

$$t_f = 200\, d_{50} \tag{23}$$

Taking into account that most of the displacement will be concentrated within a small portion of the overall sigmoidal "plastic" trough, Eq. (23) can be written as:

$$S_p(x) = \tanh\left(\frac{2\pi}{5\times 200\, d_{50}}x\right) \tag{24}$$

in which we assume that the shear zone of width t_f corresponds to 20% of the total width T of the "plastic" settlement trough ($T = 5t_f$). Although there is no rigorous theoretical justification for this assumption, it provides a reasonable fit with FE and centrifuge test data.

As schematically illustrated in Fig. 12, the initial shear zone, t_f, will be broadened reaching the surface due to: (a) the dilation, and (b) the fault outcropping angle. As previously mentioned, while the width of the shear zone at some depth has been systemically observed to be on the order of 10 cm, near the surface it is increased systematically to an order of 1 m (McCalpin, 1996). This manifestation of the shear zone at the surface is denoted here as the *plasticized zone*. We assume that this thickening of the shear zone is related primarily to the dilatancy of the soil, expressed through ψ. For bedrock offset h, the shear zone at the soil surface will be subjected to shearing:

$$\gamma = \frac{h - h_y}{200\, d_{50}} \tag{25}$$

where h_y is the critical offset for fault outcropping. The associated broadening can be assumed analogous to $\sin(\psi)$:

$$\frac{h - h_y}{200\, d_{50}}\sin(\psi) \tag{26}$$

and Eq. (24) can be modified accordingly:

$$S_p(x) = \tanh\left(\frac{2\pi x}{5\times 200\, d_{50}\left[1 + \dfrac{h - h_y}{200\, d_{50}}\sin(\psi)\right]}\right) \tag{27}$$

Since the fault will not outcrop vertically, its width at the surface will increase in proportion to $1/\sin(\alpha_{out})$, where α_{out} is the angle of fault outcropping. Taking into account that the fault outcrops at distance W, and in order to derive negative settlements for normal faulting and positive for reverse [tanh is symmetrical to the point (0,0)], and to finally attain the actual dislocation ($h - h_y$) instead of the default unitary value, Eq. (27) is re-written as:

$$S_p(x) = \left\{\tanh\left(\frac{2\pi}{5\times 200\, d_{50}\left[1 + \dfrac{h - h_y}{200\, d_{50}}\sin(\psi)\right]\arcsin(\alpha_{out})}(x - W)\right) - 1\right\}\frac{h - h_y}{2} \tag{28}$$

for normal faulting, and

$$S_p(x) = \left\{1 - \tanh\left(\frac{2\pi}{5\times 200\, d_{50}\left[1 + \dfrac{h - h_y}{200\, d_{50}}\sin(\psi)\right]\arcsin(\alpha_{out})}(x - W)\right)\right\}\frac{h - h_y}{2} \tag{29}$$

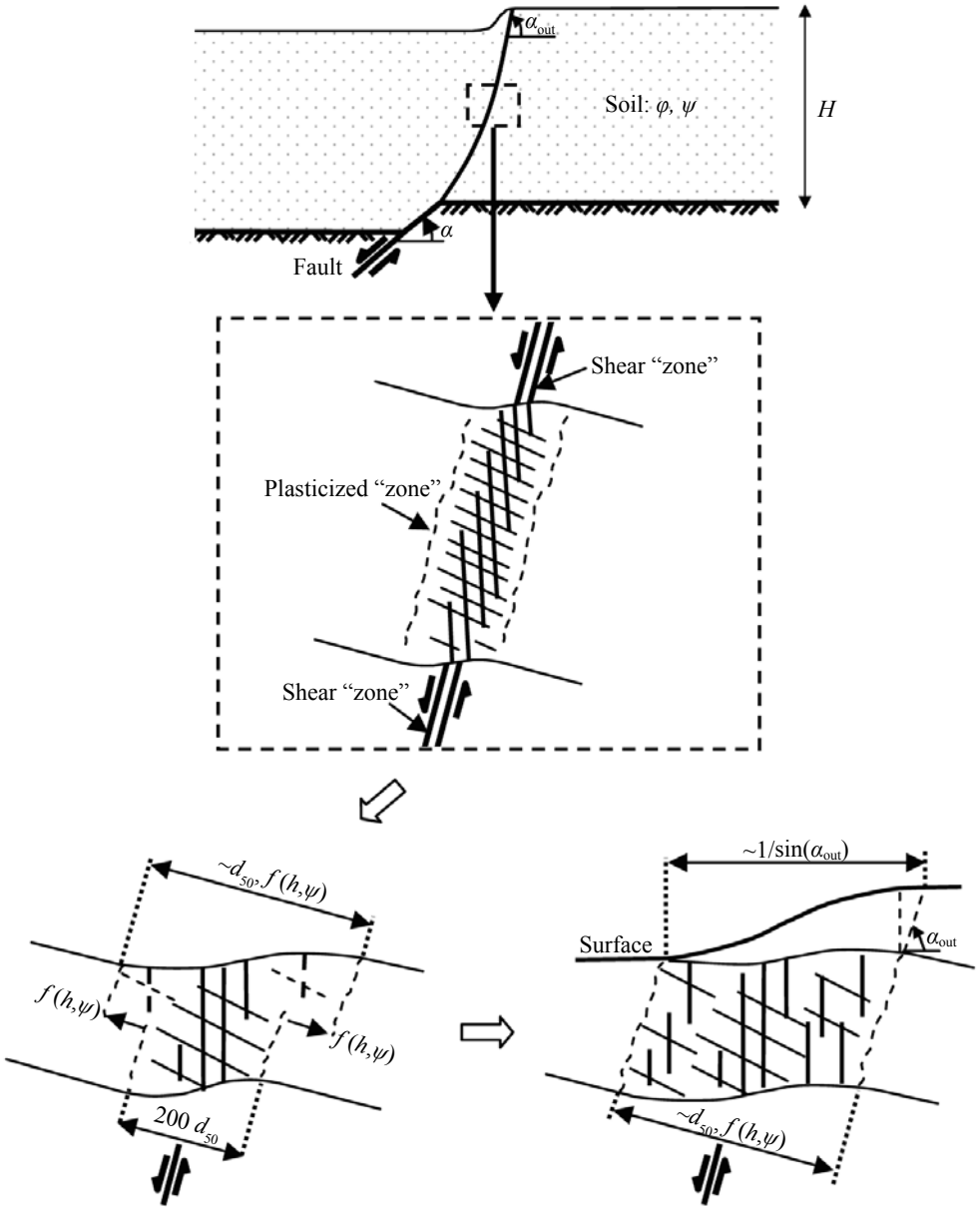

Fig. 12 Methodology for estimation of the "plastic" part of the displacement trough: width of plasticized zone as a function of φ, ψ, h/H, and α

for reverse faulting.

The outcropping location W can be evaluated from Eqs. (5) and (9), for normal and thrust faulting, respectively; the outcropping dip angle α_{out} can be evaluated on the basis of Eqs. (4) and (8):

$$\alpha_{out} = \arctan\left(\frac{\mathrm{d}}{\mathrm{d}z}\left[\frac{z}{H}\tan(45^{\circ} - \varphi/2)\bullet \exp\left(\frac{1}{\cos(\pi-\alpha)}\,\frac{9}{2\pi^2}\,\tan(\psi)\frac{z}{H}\right)\right]\right\}_{z/H=1} \quad (30)$$

for normal faulting, and

$$\alpha_{out} = \arctan\left(\frac{\mathrm{d}}{\mathrm{d}z}\left[\frac{z}{H}\tan(45^{\circ} - \varphi/2)\bullet \exp\left(\cos(\alpha)\,\frac{3\pi}{2}\,\tan(\psi)\frac{z}{H}\right)\right]\right\}_{z/H=1} \quad (31)$$

for thrust faulting.

3.3 Additional displacement due to formation of fault graben

As already discussed, for normal faulting at $\alpha \le 45^{\circ} + \psi/2$ a secondary antithetic rupture develops (Lade *et al*., 1984), leading to formation of a gravity graben and

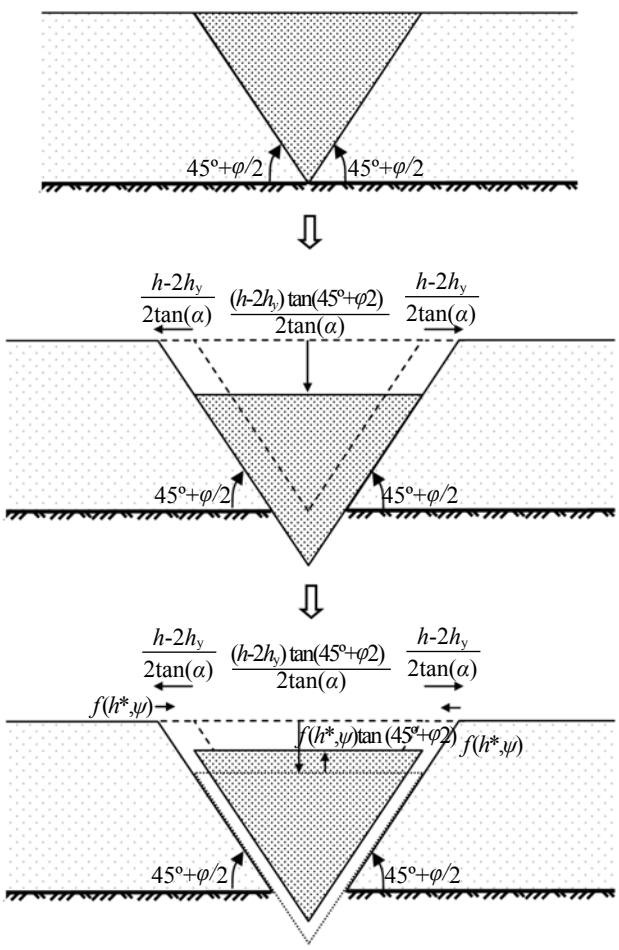

Fig. 13 Estimating the additional vertical surface depression due to formation of a fault graben, as a function of φ, ψ, h/H, and α

amplification of the vertical displacement trough. The secondary antithetic rupture can be seen to be analogous to a wall under active conditions, but to the opposite direction of the wall representing the main rupture (see also Fig. 2). FE analysis results (Anastasopoulos *et al.*, 2007a) indicate that the secondary rupture starts propagating only after the main rupture has outcropped (i.e., for $h > h_y$), and emerges at the ground surface when the bedrock displacement reaches a value $h_{y,2}$ which is roughly two times larger than h_y:

$$h_{y,2} = 2h_y \tag{32}$$

Figure 13 illustrates the developed mechanical analogue. We make two simplifying assumptions: (i) the additional settlements associated with the development of the fault graben are solely due to horizontal extension; and (ii) both ruptures propagate to the surface at approximately $45^o + \varphi/2$. Soil response can then be divided into three distinct phases: (a) initially, for $h < h_y$, none of the ruptures has propagated all the way to the surface; (b) then, for $h_y < h < h_{y,2}$ the primary rupture has outcropped (for $h = h_y$) and all of the imposed displacement is accumulated on it; and (c) finally, for $h = h_{y,2} = 2h_y$ the secondary rupture emerges at the surface, and any additional displacement $(h - 2h_y)$ is analyzed in two opposite horizontal extensional components of magnitude $(h - 2h_y)/2\tan(\alpha)$. Ignoring soil deformability (i.e., assuming that graben and surrounding soil behave as a rigid body), for the system to maintain kinematic equilibrium, the graben will have to "fall", generating additional settlement (solely due to horizontal extension) equal to:

$$s_g = \frac{(h-2h_y)\tan(45^o+\varphi/2)}{2\tan(\alpha)} \tag{33}$$

This additional settlement is directly related to the additional deformation of the shear zone, and thus further broadening due to dilation, always in analogy to $\sin(\psi)$:

$$200\,d_{50}\left[1+\frac{(h-2h_y)\sin(\psi)}{200\,d_{50}\sin(45^o+\phi/2)}\right] \tag{34a}$$

This broadening of the shear zone will compensate for some of the imposed extension, reducing it by:

$$\frac{h-2h_y}{2\tan(\alpha)} - 200\,d_{50}\left[1+\frac{(h-2h_y)\sin(\psi)}{200\,d_{50}\sin(45^o+\phi/2)}\right] \tag{34b}$$

And therefore, the additional settlement due to the graben will be:

$$s_g = \left\{\frac{h-2h_y}{2\tan(\alpha)} - 200\,d_{50}\left[1+\frac{(h-2h_y)\sin(\psi)}{200\,d_{50}\sin(45^o+\phi/2)}\right]\right\}\cdot \tan(45^o+\varphi/2) \tag{35}$$

In conclusion, for $\alpha < 45^o+\psi/2$ and $h/2h_y$, Eq. (28) has to be modified to take account of the additional settlement due to formation of a fault graben, as follows:

$$S_p(x) = \left\{\tanh\left(\frac{2\pi}{5\times 200\,d_{50}\left[1+\frac{(h+s_g)-h_y}{200\,d_{50}}\sin(\psi)\right]\arcsin(\alpha_{out})}(x-W)\right)-1\right\}\frac{(h+s_g)-h_y}{2} \tag{36}$$

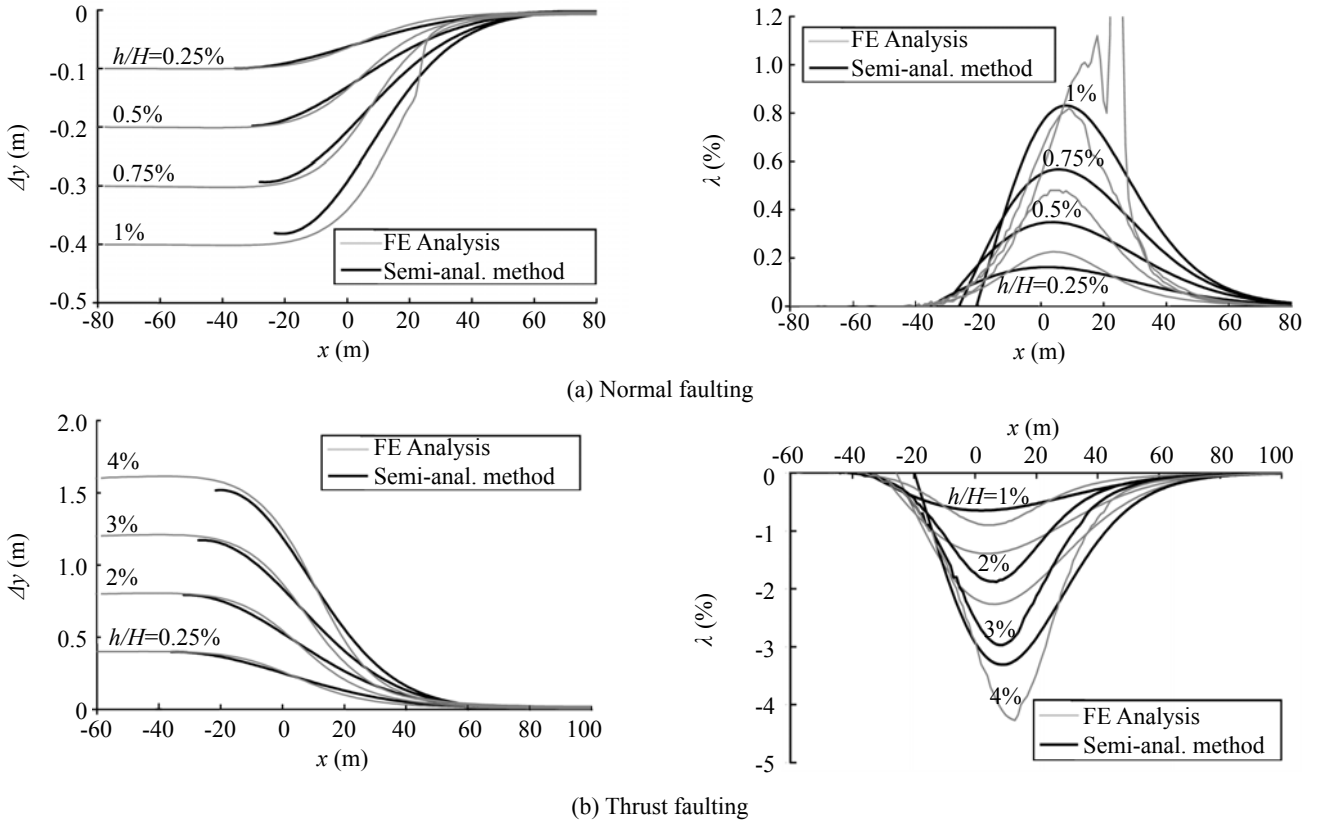

Fig. 14 Semi-analytical model for estimation of the surface displacement profile: quasi-elastic vertical displacement profile Δy and associated angular distortion λ compared to FE analysis results at $\alpha = 60^o$ through loose sand

The fault scarp height can be estimated as follows :

$$s = (h + s_g) - h_y \tag{37}$$

3.4 Results and discussion

Figure 14 compares the quasi-elastic vertical displacement trough predicted by the semi-analytical approach and calculated from of the FE analyses, for normal and thrust faulting at $\alpha = 60^o$ in loose sand. The comparison is conducted for bedrock displacement $\hat{h} \le \hat{h}_y$, so that the rupture has not yet outcropped and the quasi-elastic assumption is valid. In the case of normal faulting, the comparison between semi-analytical estimate and FE results is quite acceptable, with the most substantial difference being observed for $\hat{h} = 1\%$. This discrepancy is mainly due to the fact that the rupture has already outcropped in the FE analysis, while in the semi-analytical approach we have assumed $\hat{h}_y = 1.25\%$ (see Table 1). In thrust faulting, the comparison is also quite good.

Comparisons of the total displacement trough predicted with the semi-analytical approach with the results of FE analysis are shown in Figs. 15 to 18. The semi-analytical estimate compares well with FE analysis results in the case of normal faulting at $\alpha = 60^o$ (Fig. 15). Both the predicted quasi-elastic and the plastic part of displacement compare well with FE analysis results, the fault scarps are about equal to the FE analysis, and the location of fault outcropping is estimated correctly. The main discrepancy lies in the curving of the soil surface around the location of the fault outcrop. At this region, even after the rupture has outcropped, the soil continues deforming quasi-elastically. Given the assumption that quasi-elastic deformation takes place only before the rupture reaches the surface, this cannot be predicted using this simplified method.

Figure 16 depicts the comparison for normal faulting at 45°. Although the comparison is conducted only for the primary rupture, the same procedure could be applied for the secondary rupture, as well. In both types of sand (dense and loose), the semi-analytical approach slightly underestimates the fault scarp s and the maximum settlement. On the other hand, and as for $\alpha = 60^o$, the location of fault outcropping is predicted accurately.

The comparison for thrust faulting at 60° is illustrated in Fig. 17. In dense sand, the comparison with FE results is quite acceptable with regard to the location of the fault outcrop, as well as in terms of magnitude of fault scarp. The latter is slightly underestimated. As for normal faulting, the main difference is the curvature of the soil surface just on the hanging wall side of the fault scarp. Now, due to horizontal compression, which has been neglected in the semi-analytical model, the differences

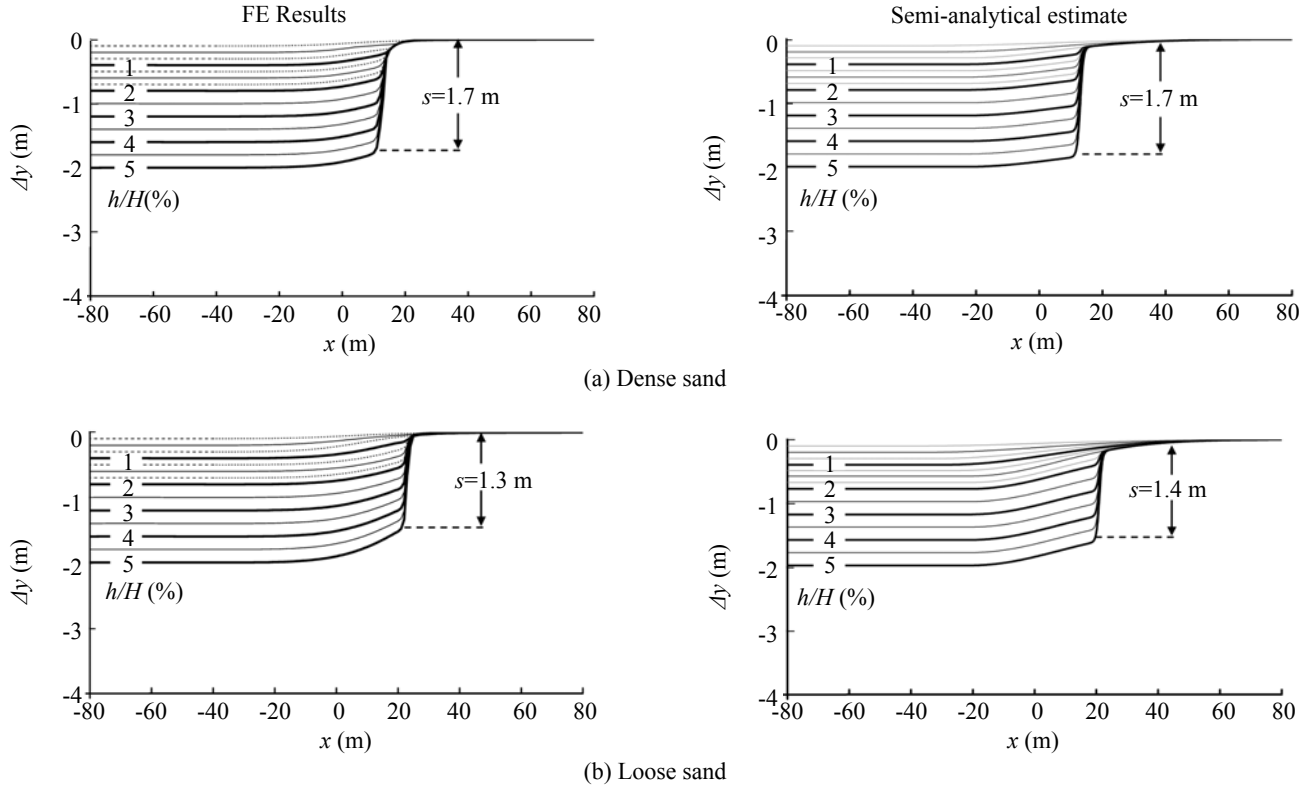

Fig. 15 Surface displacement profiles: comparison between FE results and model estimates. Normal faulting at α = 60º

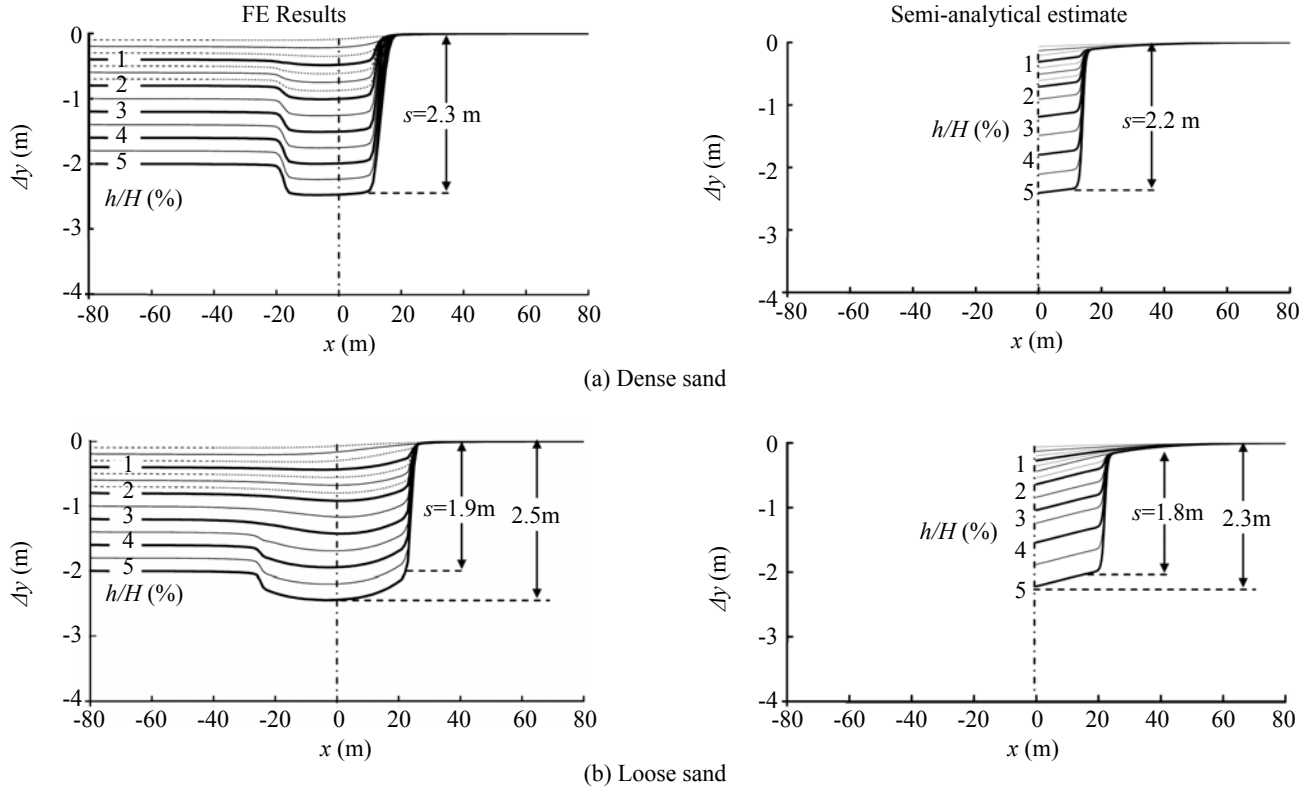

Fig. 16 Surface displacement profiles: comparison between FE results and model estimates. Normal faulting at α = 45º

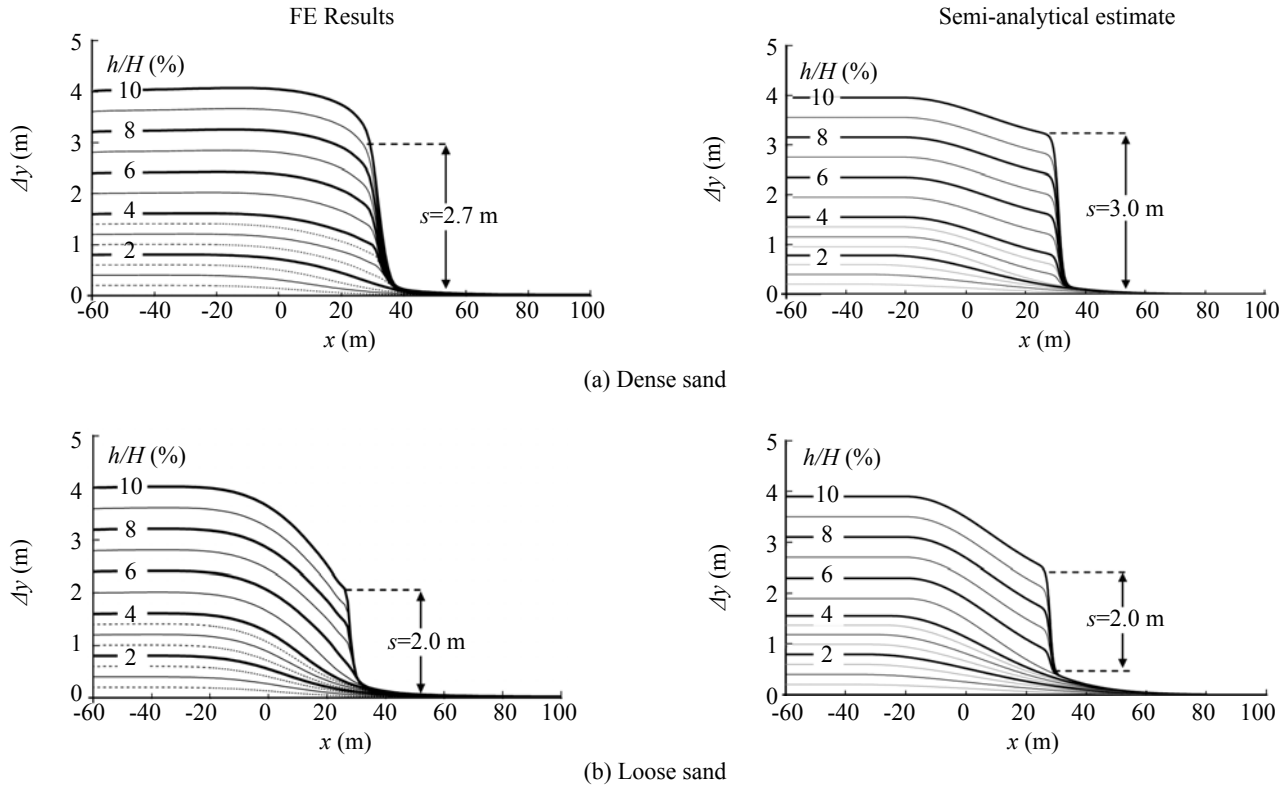

Fig. 17 Surface displacement profiles: comparison between FE results and model estimates. Thrust faulting at α = 60°

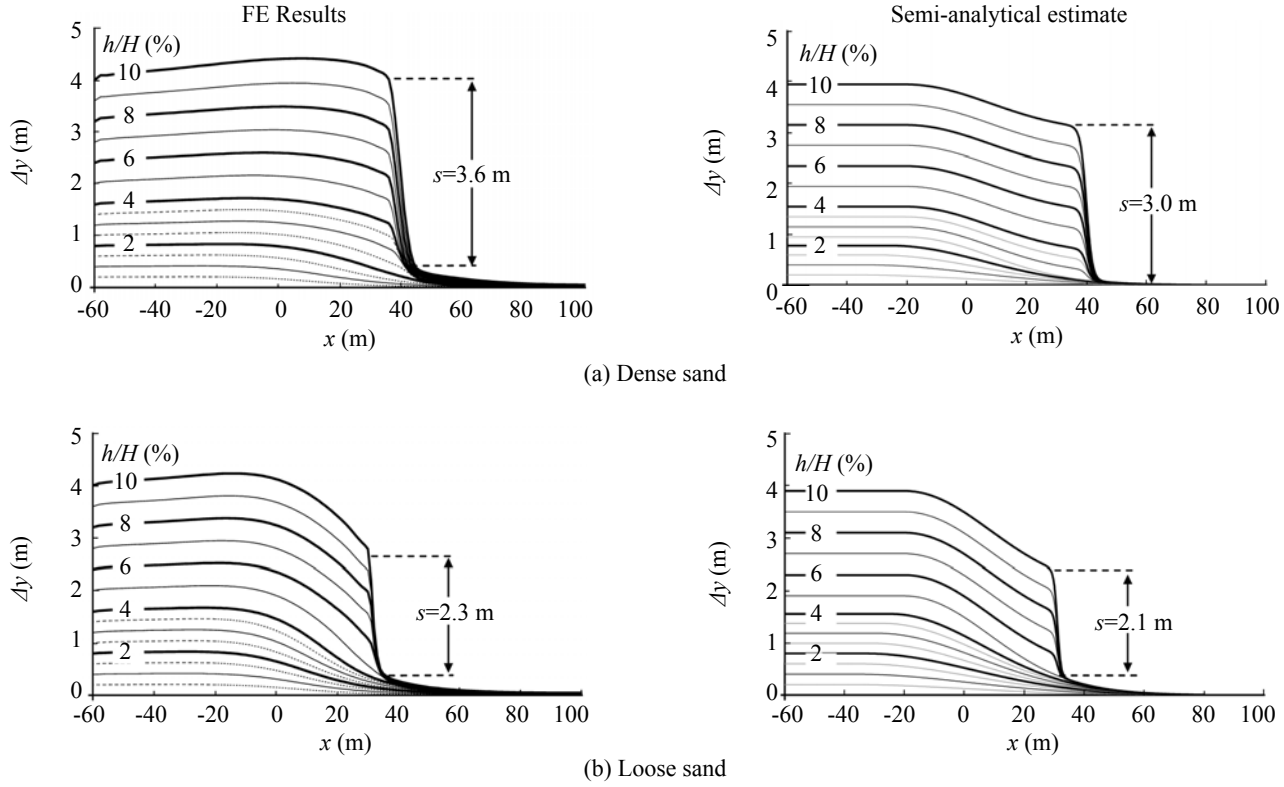

Fig. 18 Surface displacement profiles: comparison between FE results and model estimates. Thrust faulting at α = 45°

are more pronounced. The compression magnifies the effect of dilation. The results for loose sand tend to confirm the hypothesis: the difference between FE analysis and the semi-analytical model are much less significant.

Finally, as illustrated in Fig. 18 the differences become a little more significant in the case of thrust faulting at 45°. As in the previous cases, the location of fault outcropping is estimated accurately. However, the effect of horizontal compression (neglected in the semi-analytical model) is now more substantial, leading to more intense bulging of the soil surface just on the hanging wall side of the fault scarp. As a result, the vertical displacement at the surface is amplified, becoming larger than the imposed bedrock offset (4.3 m instead of 4 m) in the FE analysis. The semi-analytical approach cannot predict such response: the effect of horizontal compression has been neglected. As a result, it underestimates the fault scarp by about 15%. The discrepancy is less important in loose sand (the dilation is lower).

4 Conclusions and limitations

The main conclusions of our study are as follows:

(1) The semi-analytical expressions developed for estimation of the rupture path provide a useful tool for a first comparative estimation of the seismic hazard of a given area. However, to reliably estimating the exact outcropping location is a task with inherent uncertainty, and therefore the results of the proposed method should be treated with caution.

(2) The semi-analytical method for estimating of the displacement profile distinguishes between quasi-elastic and plastic deformations. The quasi-elastic trough refers to the ground settlement before fault outcropping, while the plastic arises after fault outcropping.

(3) The methodology presented herein is based on simple mechanistic models with empirical additions based on geotechnically meaningful parameters. Thus, it can be easily modified by the user, if different data is to be utilized. The method has been validated against the results of FE analysis (Anastasopoulos *et al*., 2007a) and some centrifuge model test results (Bransby *et al*., 2007a; 2007b).

The work presented herein provides only an approximate estimate of complex soil response. Several simplifying assumptions have been made, and the realism of the presented results should be viewed with caution. Specifically: (i) neglecting the horizontal component of motion is not always a realistic assumption, especially for low angle reverse (i.e. thrust) faulting; and (ii) the sand has been assumed to be dry. In real conditions, a water table may be present, and the response may be altered due to generation of transient excess pore water pressures or different effective stress conditions (Johansson & Konagai, 2006; 2007).

The estimation of the location of fault outcropping at the ground surface, relies on its location at bedrock, which is not at all straight-forward in the field. Even if the fault line is depicted with clarity in a large−scale map, there is no practical guarantee that the fault will "break" exactly at the same location in future possible earthquakes. Thus, infrastructure analyses should be repeated for a range of postulated possible fault break positions.

Acknowledgements

This work was funded by OSE (the Greek Railway Organization), as part of the research project "Railway Bridges on Active Seismic Faults." Centrifuge testing and finite element analyses formed part of the EU research project "QUAKER", funded through the EU Fifth Framework Programme, under contract number: EVG1-CT-2002-00064.

References

Anastasopoulos I and Gazetas G (2007a), "Foundation-Structure Systems over a Rupturing Normal Fault: Part I. Observations After the Kocaeli 1999 Earthquake," *Bulletin of Earthquake Engineering*, **5**(3): 253-275.

Anastasopoulos I and Gazetas G (2007b), "Behaviour of Structure–Foundation Systems over a Rupturing Normal Fault: Part II. Analysis of the Kocaeli Case Histories," *Bulletin of Earthquake Engineering,* **5**(3): 277-301.

Anastasopoulos I, Gazetas G, Bransby MF, Davies MCR and El Nahas A (2007a), "Fault Rupture Propagation through Sand: Finite Element Analysis and Validation through Centrifuge Experiments," *Journal of Geotechnical and Geoenvironmental Engineering,* **133**(8): 943-958.

Anastasopoulos I, Gazetas G, Bransby MF, Davies MCR and El Nahas A (2007b), "Normal Fault Rupture Interaction with Strip Foundations," *Journal of Geotechnical and Geoenvironmental Engineering* (submitted for possible publication).

Anastasopoulos I, Gerolymos N, Gazetas G and Bransby MF (2008), "Simplified Approach for Design of Raft Foundations Against Fault Rupture. Part II: Soil–Structure Interaction, Companion Paper," *Soils and Foundations* (submitted for possible publication).

Berill JB (1983), "Two-dimensional Analysis of the Effect of Fault Rupture on Buildings with Shallow Foundations," *Soil Dynamics and Earthquake Engineering,* **2**(3): 156-160.

Bernard P, Gariel J-C and Dorbath L (1997), "Fault Location and Rupture Kinematics of the Magnitude 6.8, 1992 Erzincan Earthquake, Turkey, from Strong Ground Motion and Regional Records," *Bulletin of the Seismological Society of America*, **87**(5): 1230-1243

Bransby MF, Davies MCR and El Nahas A (2007a), "Centrifuge Modelling of Normal Fault-foundation

Interaction," *Bulletin of Earthquake Engineering,* Special Issue: Integrated Approach to Fault Rupture- and Soil-foundation Interaction, Companion paper (submitted for possible publication).

Bransby MF, Davies MCR and El Nahas A (2007b), "Centrifuge Modelling of Reverse Fault-foundation Interaction," *Bulletin of Earthquake Engineering,* Special Issue: Integrated Approach to Fault Rupture- and Soil-foundation Interaction, Companion paper (submitted for possible publication).

Bray JD (1990), "The Effects of Tectonic Movements on Stresses and Deformations in Earth Embankments," *Ph.D. Dissertation*, University of California, Berkeley.

Bray JD, Seed RB, Cluff LS and Seed HB (1994), "Earthquake Fault Rupture Propagation through Soil," *Journal of Geotechnical Engineering*, ASCE, **120**(3): 543-561.

Cole DA Jr and Lade PV (1984), "Influence Zones in Alluvium Over Dip-slip Faults," *Journal of Geotechnical Engineering*, ASCE, **110**(5): 599-615.

Duncan JM and Lefebvre G (1973), "Earth Pressure on Structures Due to Fault Movement," *Journal of Soil Mechanics and Foundations Division, ASCE,* **99**(SM12): 1153-1163.

El Nahas A, Bransby MF and Davies MCR (2006), "Centrifuge Modelling of the Interaction Between Normal Fault Rupture and Rigid, Strong Raft Foundations," *Proc. International Conference on Physical Modelling in Geotechnics*, Hong Kong, August, pp. 337-342.

Faccioli E, Anastasopoulos I, Callerio A and Gazetas G (2007), "Case Histories of Fault–foundation Interaction," *Bulletin of Earthquake Engineering,* Special Issue: Integrated Approach to Fault Rupture- and Soil-foundation Interaction, Companion paper (submitted for possible publication).

Gaudin C (2002), "Experimental and Theoretical Study of the Behaviour of Supporting Walls: Validation of Design Methods," *Ph.D. Dissertation*, Laboratoire Central des Ponts et Chaussées, Nantes, France.

Hvorslev MJ (1960), "Physical Components of the Shear Strength of Saturated Clays," *Proc. Res. Conf. Shear Strength of Cohesive Soils, American Society of Civil Engineers*, pp. 437-501.

Johansson J and Konagai K (2006), "Fault Induced Permanent Ground Deformations—An Experimental Comparison of Wet and Dry Soil and Implications for Buried Structures," *Soil Dynamics & Earthquake Engineering*, **26**(1): 45-53.

Johansson J and Konagai K (2007), "Fault Induced Permanent Ground Deformations: Experimental Verification of Wet and Dry Soil, Numerical Findings' Relation to Field Observations of Tunnel Damage and Implications for Design," *Soil Dynamics & Earthquake Engineering*, **27**(10): 938-956.

Lade PV, Cole DA Jr and Cummings D (1984), "Multiple Failure Surfaces Over Dip-slip Faults," *Journal of Geotechnical Engineering*, ASCE, **110**(5): 616-627.

Lambe TW (1973), "Predictions in Soil Engineering," *Géotechnique*, **23**(2): 149-202.

Lazarte CA (1996), "The Response of Earth Structures to Surface Fault Rupture," *Ph.D. Dissertation*, University of California, Berkeley.

Lazarte CA, Bray JD, Johnson AM and Lemmer RE (1994), "Surface Breakage of the 1992 Landers Earthquake and its Effects on Structures," *Bulletin of the Seismological Society of America*, **84**: 547-561.

Lee JW and Hamada M (2005), "An Experimental Study on Earthquake Fault Rupture Propagation Through a Sandy Soil Deposit," *Journal of Structural Mechanics and Earthquake Engineering*, JSCE, **22**(1): 1-13.

Matsuda T (1974), "Surface Faults Associated with Nobi (Mino-Owari) Earthquake of 1891, Japan," *Spec. Bull. Earthquake. Res. Inst.*, Univ. Tokyo, **13**: 85-126.

McCalpin JP (1996), *Paleoseismology*, Academic Publishers, New York.

Morgenstern NR and Tchalenko JS (1967), "Microscopic Structures in Kaolin Subjected to Direct Shear," *Geotechnique*, **17**: 309-328.

Muir Wood D (2002), "Some Observations of Volumetric Instabilities in Soils," *International Journal of Solids and Structures*, **39**: 3429-3449.

Nakai T, Muir Wood D and Stone KJL (1995), "Numerical Calculations of Soil Response over a Displacing Basement," *Soils and Foundations*, **35**(2): 25-35.

Nakata T, Tsutsumi H, Punongbayan RS, Rimando RE, Daligdig JA, Daag AS and Besana GM (1996), "Surface Fault Ruptures of the 1990 Luzon Earthquake, Philippines," *Special Publication No.25*, Research Center for Regional Geography, Hiroshima Univ..

Peck RB (1969), "Deep Excavations and Tunnelling in Soft Ground," *State-of-the-art Volume*, *Proceedings 7th International Conference on Soil Mechanics and Foundations,* Mexico City.

Philip H, Rogozhin E, Bousquet JC and Borisov B (1992), "The Armenian Earthquake of 1988 December 7: Faulting and Folding, Neotectonics and Palaeoseismicity," *Geophysical Journal International*, **110**(1): 141-158.

Prucha JJ, Graham JA and Nickelsen RP (1965), "Basement-Controlled Deformation in Wyoming Province of Rocky Mountains Foreland," *Bulletin of the American Association of Petroleum Geologists*, **49**(7): 966-992.

Rankin WJ (1988), "Ground Movements Resulting from Urban Tunnelling," *Proceedings of the Conference of Engineering Geology and Underground Movements,* Nottingham, pp. 79-92.

Roscoe KH (1970), "The Influence of Strains in Soil Mechanics," 10th Rankine Lecture, *Geotechnique*, **20**(2): 129-170.

Roth WH, Sweet J and Goodman RE (1982), "Numerical and Physical Modelling of Flexural Slip Phenomena and Potential for Fault Movement," *Rock Mechanics,* Suppl. **12**: 27-46.

Segall P and Lisowski M (1990), "Surface Displacements in the 1906 San Francisco and 1989 Loma Prieta Earthquakes," *Science*, **250**(4985): 1241-1244.

Sibson RH (2003), "Thickness of the Seismic Slip Zone," *Bulletin of the Seismological Society of America*, **93**(3): 1169-1178.

Tchalenko JS (1970), "Similarities Between Shear Zones of Different Magnitudes," *Bulletin of the Geological Society of America*, **81**: 1625-1640.

Vardoulakis I, Graf B and Hettler A (1985), "Shear-band Formation in a Fine Grained Sand," *Proc. 5th International Conference of Numerical Methods in Geomechanics*, Nagoya, Rotterdam: Balkema, pp. 517-522.

Wells DL and Coppersmith KJ (1994a), "New Empirical Relationships Among Magnitude, Rupture Length, Rupture Width, Rupture Area and Surface Displacement," *Bulletin of the Seismological Society of America,* **84**(4): 974-1002.

Wells DL and Coppersmith KJ (1994b), "New Empirical Relationships among Magnitude, Rupture Length, Rupture Width, Rupture Area and Surface Displacement," *Bulletin of the Seismological Society of America,* **84**(4): 974-1002

Youd, T. L. (1989), "Ground Failure Damage to Buildings During Earthquakes," *Foundation Engineering—Current Principles and Practices*, Vol. 1, New York: ASCE, pp. 758-770.